THE ASTROPHYSICAL JOURNAL, 421:L19–L22, 1994 January 20

ROSAT OBSERVATIONS OF VRO 42.05.01

DAVID N. BURROWS AND ZHIYU GUO
Department of Astronomy and Astrophysics, The Pennsylvania State University, 525 Davey Laboratory, University Park, PA 16802;
e-mail: I: burrows@astro.psu.edu
Received 1993 August 11; accepted 1993 October 26

ABSTRACT

We present the first X-ray images and spectra of the unusual supernova remnant VRO 42.05.01, based on a 22,680 s observation of the remnant with the *ROSAT* PSPC. The overall shape of the X-ray remnant is similar to that of the radio remnant, but the X-ray morphology differs from the radio morphology in that the X-ray emission is not edge-brightened. The X-ray data are consistent with an isothermal remnant with variations in absorbing column density across the remnant that probably account for some of the observed structure. The remnant has an X-ray temperature of $\sim 8.5 \times 10^6$ K and an absorbing column of a few times 10^{21} cm^{-2}. This absorbing column is surprisingly small for the nominal distance of 5 kpc, and requires a low mean density along this line of sight.

Subject headings: ISM: individual (VRO 42.05.01) — supernova remnants — X-rays: ISM

1. INTRODUCTION

VRO 42.05.01 (G166.0+4.3) has been identified as a supernova remnant on the basis of its nonthermal radio spectrum, optical line ratios, and high-velocity optical filaments (van den Bergh 1960; Haslam & Salter 1971; Lozinskaya 1975, 1979; D'Odorico & Sabbadin 1977). Aperture synthesis radio observations (Landecker et al. 1982; Pineault, Landecker, & Routledge 1987) reveal an unusual morphology, with a northeastern circular component (the "shell") intersected by a much larger bowl-shaped component in the southwest (the "wing" component). The morphology suggests that this supernova remnant has broken out of the cloud within which it formed, expanded across an interstellar tunnel or cavity, and is now encroaching on the material that forms the opposite tunnel wall (Pineault et al. 1987). In fact, it bears a remarkable resemblance to models of such remnants by Tenorio-Tagle, Bodenheimer, & Yorke (1985). Based on the radio Σ-D-z relationship, Landecker et al. (1982) obtain a distance of 5 kpc, from which Pineault et al. (1987) derive an age of 81,000 yr, a shell radius of 25 pc, and a shell shock velocity of 130 km s^{-1}. No radio or optical stellar remnant has been detected.

Optical observations find line ratios in the optical filaments of VRO 42.05.01 characteristic of supernova remnants (Fesen, Blair, & Kirshner 1985; Pineault et al. 1985) and a filamentary structure similar to that observed in the radio continuum (Fesen, Gull, & Ketelsen 1983; Pineault et al. 1985). Shock velocities of over 100 km s^{-1} are implied by optical line ratios and velocities (Fesen et al. 1983; Lozinskaya 1979).

The only published X-ray detection of VRO 42.05.01 was by the *HEAO 1* A-1 experiment, which measured a flux of 0.0050 ± 0.0013 counts cm^{-2} s^{-1} over the band 0.5–25 keV for the source 1H 0529+427 (Wood et al. 1984). VRO 42.05.01 was not observed by *Einstein*, and the *EXOSAT* observation has not been published.

2. OBSERVATION AND DATA ANALYSIS

Our data were obtained with the *ROSAT* Position Sensitive Proportional Counter (PSPC) between 1991 March 5 and March 25 (during AO 1). The total observation time was 22,680 s. Figure 1 shows the count rate over the PSPC field of view versus time for this observation. The count rate shows a relatively stable lower level of 6–8 counts s^{-1} with large increases due to scattered solar X-rays near the beginning of most observing intervals (OBIs). Although we have developed data reduction procedures for eliminating much of this contamination from images (Snowden et al. 1994), we have not yet developed analogous cleaning procedures applicable to spectral data. In order to minimize spectral contamination of these data, we have simply eliminated time intervals when the average rate exceeded ~ 7.5 counts s^{-1} (shown in black in Fig. 1). After elimination of the severely contaminated data, 9192 s of "clean" data remain. The average exposure over the supernova remnant (SNR) is about 6800 s (taking vignetting, rib obscuration, and other effects into account).

Our raw image of VRO 42.05.01 is shown in Figure 2 (Plate L1). This image was made in a broad band covering 0.52–2.02 keV and peaking at 1.2 keV (*ROSAT* bands R4–R7; see Snowden et al. 1994 for PSPC band definitions). The energy response of this band is shown in Figure 3. This observation was a victim of an unfortunate alignment of PSPC rib shadows close to the edge of remnant in several locations. The northwest and southeast outer ribs, which are nearly aligned with the straight northeastern boundary of the wing component, were unaffected by the spacecraft "wobble" (which was along these ribs), leaving an impression that this boundary may be an instrumental artifact. However, these ribs do not extend into the central 20′ of the image where the SNR is brightest. Similarly, the dark shadows along the northeast and southwest portions of the circular central rib, where this rib was tangent to the "wobble" direction, are located well outside of the SNR and do not affect our observation. We are convinced that our image of VRO 42.05.01 is unaffected by the PSPC ribs except for small regions near ($5^h25^m13^s$, $+43°15'$) and ($5^h28^m12^s$, $+42°27'$).

In order to study the diffuse emission from this SNR, we removed point source contributions and flattened the raw image using energy-dependent exposure maps as discussed by Snowden et al. (1994). The resulting flat-fielded X-ray image is shown in Figure 4 (Plate L2), smoothed with a 2.5 (FWHM) Gaussian for display purposes and overlaid with a 1420 MHz radio continuum map provided by T. Landecker (an updated version of the map presented in Pineault et al. 1987, precessed

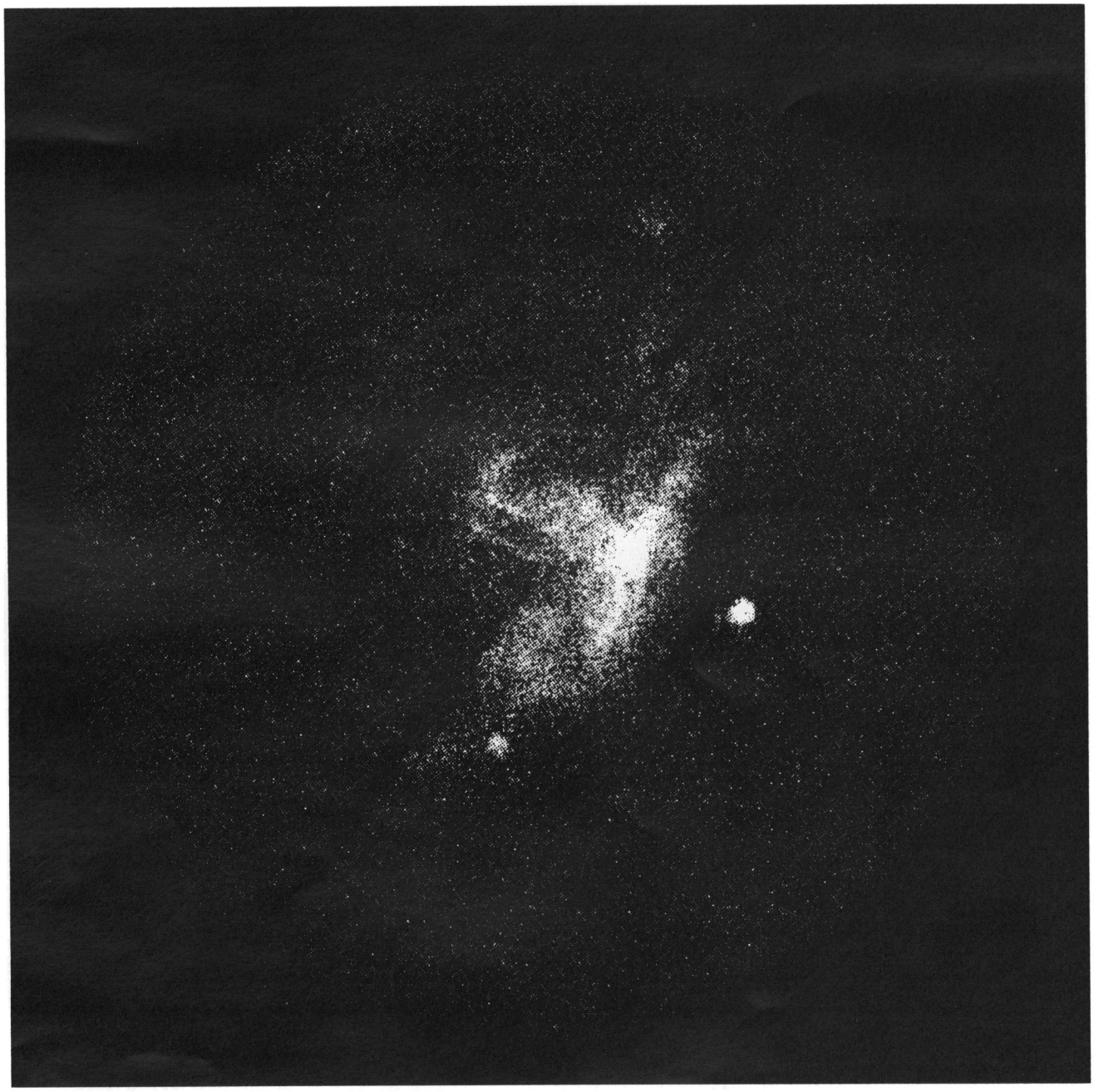

FIG. 2.—*ROSAT* PSPC raw image of VRO 42.05.01 in the R4–R7 band (energy range 0.52–2.02 keV). The X-ray image contains 25,219 photons.

BURROWS & GUO (see 421, L19)

PLATE L2

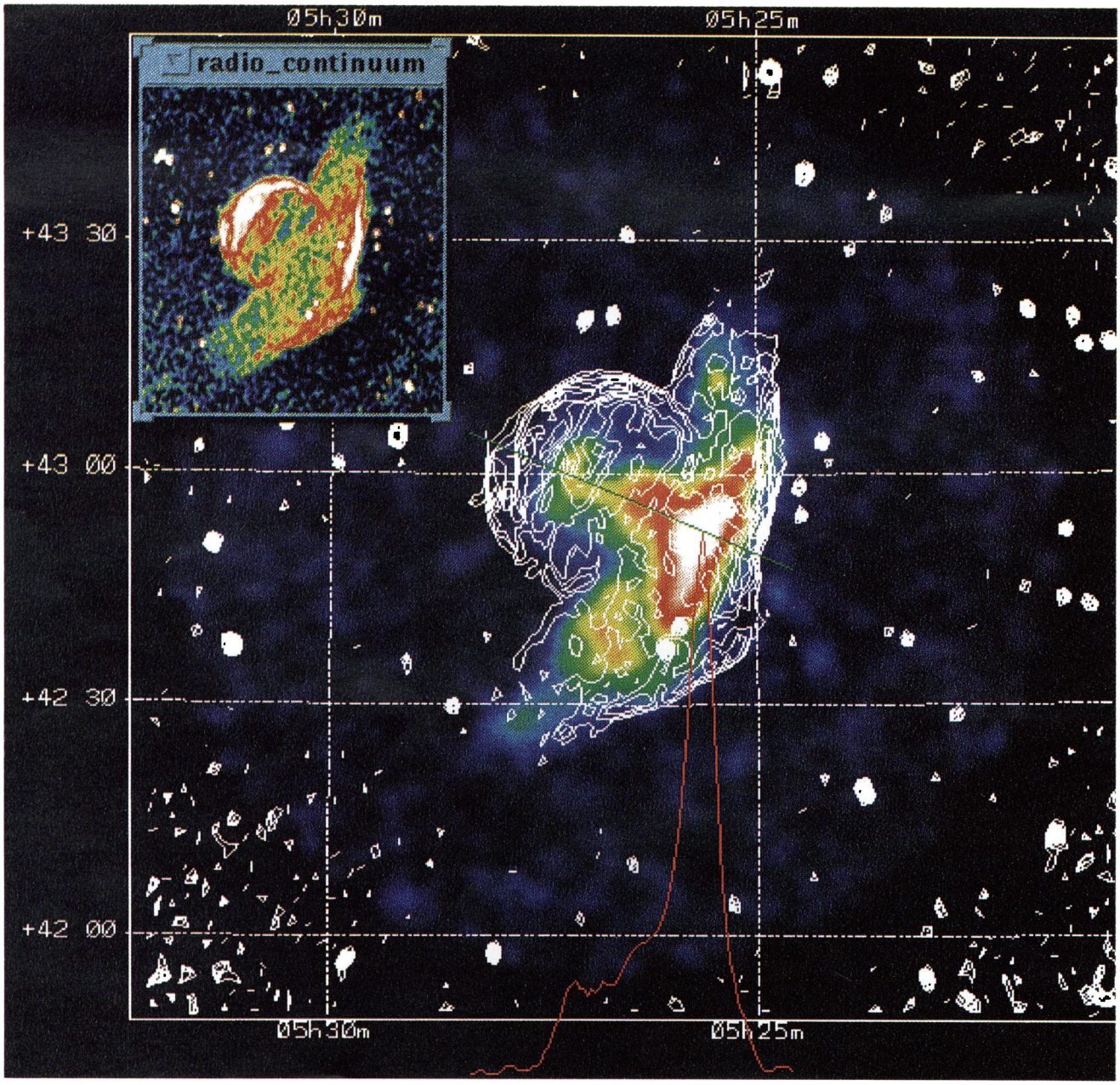

FIG. 4.—Processed image of VRO 42.05.01 in the R4–R7 band. The image of Fig. 2 has been cleaned of noncosmic contamination and point-source contributions, flattened, and smoothed with a 2.5 (FWHM) Gaussian. The coordinates are equatorial (J2000). The X-ray image is overlaid with 1420 MHz radio continuum contours (T. Landecker). The color scale for the X-ray image is logarithmic and ranges from 0 to 0.0073 counts s^{-1} $arcmin^{-2}$. The radio contours are linear and range from 0.5 to 10.25 K at intervals of 0.25 K. The red curve along the bottom of the image represents the X-ray intensity along the slice shown as a green line, which runs from ($5^h28^m23^s.5$, 43°05′07″) to ($5^h24^m36^s.8$, 42°47′37″), passing through the center of the SNR near its plane of symmetry. The inset in the upper left-hand corner is a color image of the radio continuum data, scaled from 0 to 1.67 K.

BURROWS & GUO (see 421, L19)

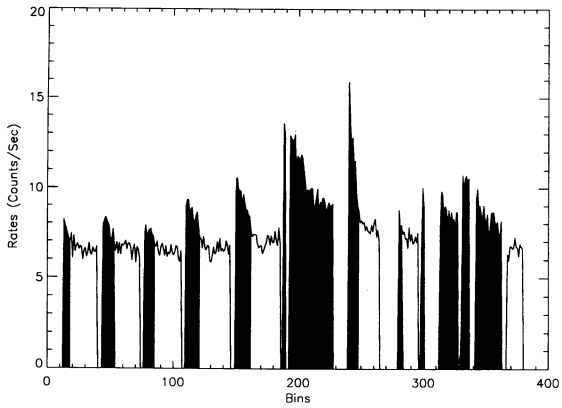

FIG. 1.—Light curve of our PSPC image of VRO 42.05.01, from the housekeeping AE ("accepted event") rate over the entire field of view. The observation intervals (OBIs) have been compressed in this figure. Time intervals highlighted in black were deleted from processing because of high count rates that indicate contamination of the data.

to J2000 coordinates and reprojected to match the *ROSAT* image). Although there is X-ray emission covering most of the radio remnant, there are important differences in the spatial distribution of the emission in these two bands. The radio image is prominently edge-brightened, both in the shell component and in the wing component. The X-ray emission nearly fills the radio shell but is not edge-brightened. It is dominated by a bright spot in the wing component, just inside the brightest radio feature along the western boundary. By analogy to the Eastern Bright Knot of Puppis A, this "Western Bright Knot" in VRO 42.05.01 may represent the interaction of the shock front with a cloud, perhaps composed of a "plug" produced during the breakout of the shock front. This interpretation is supported by the positional coincidence of this X-ray feature with a neutral cloud observed at 21 cm at velocities between -42 and -52 km s^{-1} (feature K of Landecker et al. 1989), which may be a shocked portion of the wall of a cavity within which the supernova occurred. The lack of an X-ray shell may be explained by evaporation of engulfed clouds (White & Long 1991, hereafter WL91) in the interior of the remnant, although the low internal density derived from our X-ray data argues against substantial cloud evaporation. The spatial structure in the X-ray emission of the shell component may be due to nonuniform absorption by patchy clouds of neutral material, perhaps associated with the cloud within which the supernova presumably occurred. This is consistent with the observation that the neutral column density is larger toward the shell component than toward the wing component. There is no evidence in our PSPC image for the hot tunnel postulated by Pineault et al. (1987) or for the cavity found by Landecker et al. (1989); however, this is not surprising given the large absorbing column which represents 20–30 optical depths to the $\frac{1}{4}$ keV emission expected from such a tunnel. The size of the X-ray remnant is 0.21 square degrees.

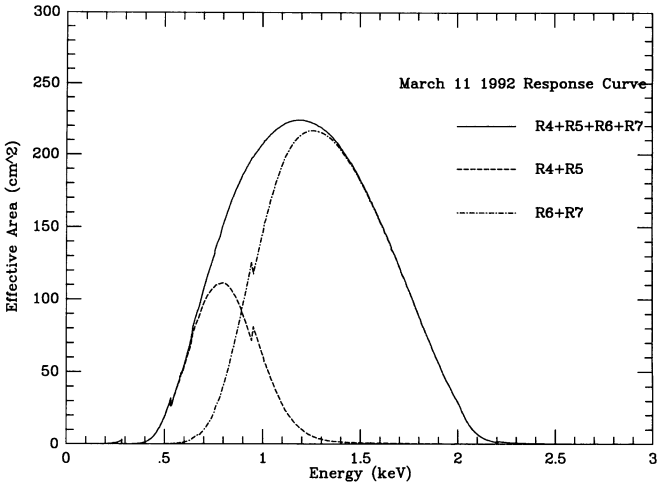

FIG. 3.—Effective area curves for the energy bands used here. These curves are derived from the DRM.06 (1992 March 11) response matrix of the *ROSAT* PSPC.

In order to look for spectral variations across the remnant, we made a "soft" image using photons with pulse height in *ROSAT* bands (R4 + R5) and a "hard" image using photons in *ROSAT* bands (R6 + R7). A map of the hard:soft ratio is shown in Figure 5 (Plate L3), overlaid with the radio contours. The most notable feature of this image is the central "hot spot" at about ($5^h26^m25^s$, $+42°56'$), indicating a hardening of the spectrum in the center of the remnant relative to the bulk of the remnant. This hot spot extends from the center of the shell component toward the wing component and is offset from the region of brightest X-ray emission. The hot spot is most easily explained by a hot interior near the center of the explosion where the low density results in a long cooling time. The edges of the wing component also appear to be somewhat harder than the mean; this could be due to absorption by the shell, which would have large column densities near the boundary.

We have extracted background-subtracted pulse-height spectra from the shell and wing portions of the remnant and fitted them to Raymond & Smith (1977) plasma models. (Our spectral extraction was done using IRAF/PROS, but we multiplied the PROS spectra, which are not corrected for vignetting, by a factor of 1.55 to account for the actual vignetted live time averaged over the SNR in order to obtain accurate normalizations and fluxes. Spectral fits were performed using XSPEC V8.32 and the 1992 March 11 version of the PSPC B response matrix, DRM.06.) The results of our spectral fits are given in Table 1 and shown in Figure 6. The normalization constant given in this table is

$$K \equiv \frac{\int n_e^2 \, dV}{4\pi D^2} . \quad (1)$$

Confidence intervals for temperature and N_H (Fig. 7) show that the two portions of the remnant probably have different spectral characteristics, with similar temperatures but substantially different N_H. The absorption appears to be larger toward the shell component, consistent with its presumed association with the cloud within which the SNR occurred. The average column density we obtain toward the shell component is in reasonable agreement with the value (3.3×10^{21} cm^{-2}) derived from the

TABLE 1

SPECTRAL FITTING RESULTS

Region	N_H (10^{21} cm^{-2})	T (10^6 K)	K (cm^{-5})	χ^2_ν
Shell (NE)	2.6	8.6	3.0×10^{11}	0.25
Wing (SW).....	1.3	8.1	4.7×10^{11}	0.84

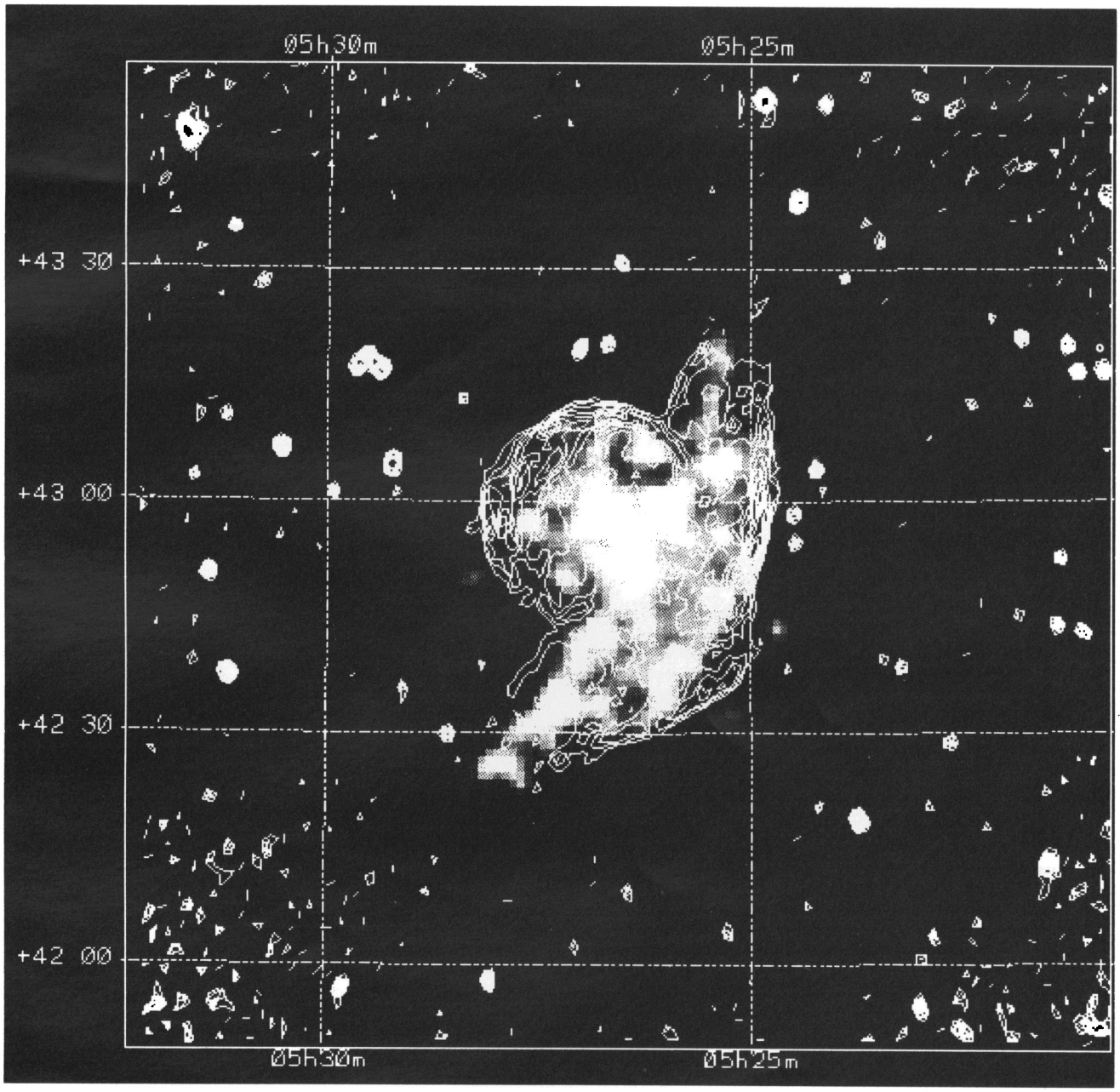

FIG. 5.—(Hard band/soft band) ratio map of VRO 42.05.01 [defined as (R6 + R7)/(R4 + R5)], overlaid with 1420 MHz radio contours. The color scale for the X-ray image is linear and ranges from 1.25 (*black*) to 3.5 (*white*).

BURROWS & GUO (see 421, L20)

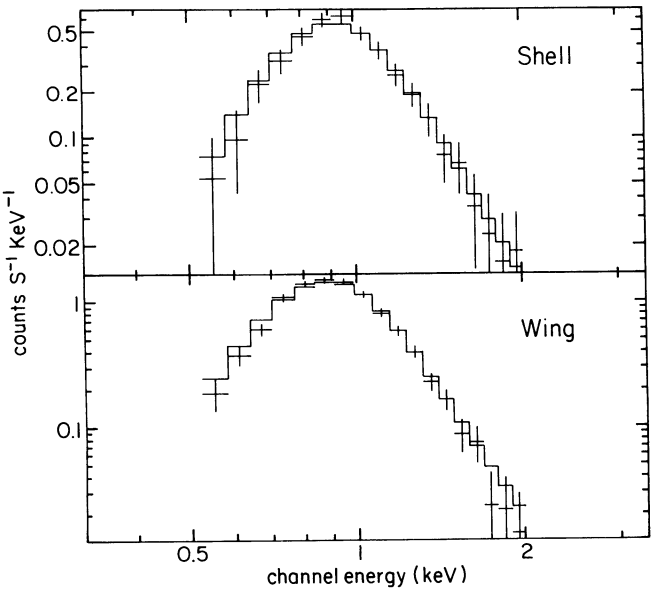

FIG. 6.—PSPC spectral fits for the two components of VRO 42.05.01. Below 0.5 keV the emission is cut off by interstellar absorption. Fit parameters are given in Table 1. *Top:* shell component; *bottom:* wing component.

extinction measurement of Fesen et al. (1985) toward the northern part of the shell.

3. DISCUSSION

The observed X-ray flux of this remnant is $F_x^{obs} \sim 9.7 \times 10^{-12}$ ergs cm^{-2} s^{-1} (0.52–2.02 keV). Corrected for interstellar absorption, we obtain a flux for the whole SNR of $F_x^{corr} \sim 1.6 \times 10^{-11}$ ergs cm^{-2} s^{-1}, where we have corrected the flux of each component for absorption by the best-fit N_H from Table 1. From the observed X-ray properties of this SNR, we use the relations given in Burrows et al. (1993) (derived primarily from Hamilton, Sarazin, & Chevalier 1983, hereafter HSC83) to obtain approximate physical parameters of this remnant, under the assumption of a spherical remnant in the adiabatic phase and assuming a distance of 5 kpc. These parameters are given in Table 2, where L_x is the X-ray luminosity from 0.52 to 2.02 keV; n_0 is the ambient density; E is the explosion energy; t is the SNR age; M_s, T_s, v_s, and R_s are the shock mass, temperature, velocity, and radius; and R_{PDS} and R_R are the radii at the onset of the pressure-driven snowplow phase and the radiative phase, respectively. We used $\Lambda - 10^{-22}$ cm^{-3} ergs s^{-1} (WL91; HSC83). To calculate the shock radius, we used an angular diameter of 0°.52, which is the size of a spherical remnant subtending the same solid angle as VRO 42.05.01. We also give physical parameters for a WL91 model of SNR evolution in a cloudy interstellar medium (ISM). In this model the fact that VRO 42.05.01 has a radio shell but a filled-center X-ray morphology is explained by evaporation of clouds in the SNR interior. The X-ray brightness distribution can be approximately fitted in the WL91 model with $\tau \gg 10$ and $C/\tau \approx 5$, where τ is the ratio of cloud evaporation time to the SNR age and C is the ratio of cloud mass to intercloud mass in the ISM.

TABLE 2

VRO 42.05.01 PHYSICAL PARAMETERS

Parameter	No Clouds (HSC83)	Clouds (WL91)	Pineault et al. 1987
d (kpc)	5	5	5
L_x (ergs s^{-1})	4.8×10^{34}	4.8×10^{34}	...
n_0 (cm^{-3})	0.011	0.0021	1.0
E (ergs)	1.4×10^{50}	2.5×10^{49}	...
t (10^3 yr)	13	24	81
M_s ($M_\odot$)	20	24	...
T_s (10^6 K)	6.6	6.6	...
v_s (km s^{-1})	680	680	130
R_s (pc)	23	23	25
R_{PDS} (pc)	54	69	...
R_R (pc)	93	113	...

The density and pressure of the SNR interior can be calculated from the normalization constant K. For a distance of 5 kpc, and assuming axial symmetry with the symmetry axis of the SNR in the plane of the sky, we calculate an approximate volume of 1.5×10^{61} cm^3. Combining this with the normalization constant K determined from our spectral fits, we obtain a mean density of 0.013 cm^{-3} and a pressure of 2.1×10^5 cm^{-3} K.

We calculate physical parameters for three distances to the SNR. As we noted above, a distance of 5 kpc was derived for VRO 42.05.01 by Landecker et al. (1982) on the basis of the radio Σ-D-z relationship. The X-ray data afford an opportunity to make an independent estimate of the distance, based on the observed absorbing column density. We assume that the best-fit column density of 1.1×10^{21} cm^{-2} toward the wing component represents the interstellar column along this line of sight, with the additional absorption toward the shell component due to the cloud within which the SNR occurred. Lucke (1978) gives an average interstellar reddening of just over 0.6 mag kpc^{-1} in the direction of VRO 42.05.01. For a standard ratio $N_H/E_{B-V} = 5.8 \times 10^{21}$ cm^{-2} mag^{-1} (Bohlin, Savage, & Drake 1978), this corresponds to a mean density of 1.1 cm^{-3}, and we obtain a distance estimate of 344 pc, considerably less than the distance based on the radio data. This distance estimate is increased, if instead of obtaining the average space density from reddening measurements, we use the distributions of $n_{H\,I}(z)$ and $n_{H_2}(z)$ given by Bloemen (1987). Integrating these distributions along the line of sight to the SNR until the observed N_H is achieved, we obtain a distance estimate of 570 pc. However, the explosion energy derived for

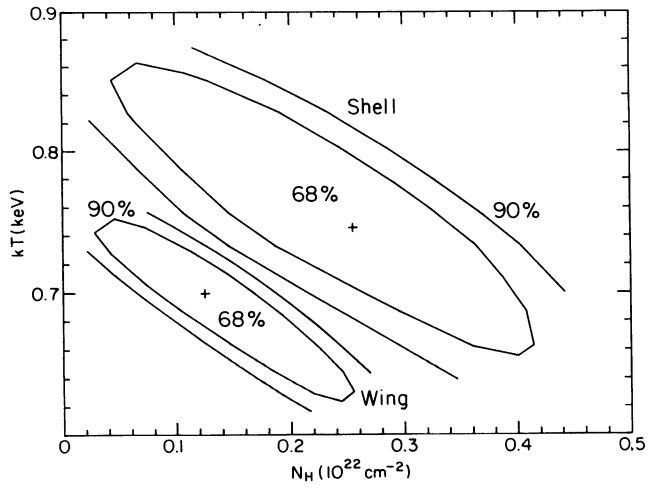

FIG. 7.—Confidence regions for spectral fits to the shell and wing components of VRO 42.05.01. Confidence levels of 68% and 90% are shown.

distances less than 1 kpc ($< 5 \times 10^{47}$ ergs for the HSC83 model) seems unreasonably small. By contrast, the physical parameters derived for 5 kpc are fairly reasonable. This suggests that the larger distance is correct, in which case this line of sight must have an unusually low average density of about 0.075 cm^{-3}. Although this is inconsistent with the average reddening determined by Lucke (1978), his data are based on Gaussian-weighted averages (10° FWHM) of reddening toward early-type stars, which are sparsely spaced on the sky. The average density over our 2° diameter field of view could therefore be much smaller than the value found by Lucke.

In Table 2 we show the values assumed or derived by Pineault et al. (1987) for comparison with our results. The initial density that we obtain from the X-ray data is considerably lower than that assumed by Pineault et al. Perhaps the low initial density suggested by the X-ray data can be understood as a result of the breakout of the SNR into a preexisting tunnel or cavity, although the cavity density estimated by Landecker et al. (1989) is still an order of magnitude larger than the density we find for the HSC83 model. However, we caution that the models we have applied here are for spherical adiabatic remnants in a uniform medium, and they may not accurately reflect the conditions in a remnant that has experienced blowout. More precise results require substantial modeling of the blowout that is beyond the scope of the present analysis.

We conclude that the PSPC spectral data for VRO 42.05.01 are consistent with a nearly isothermal remnant, in spite of its unusual morphology suggestive of breakout into a low-density phase of the ISM. The spectral variations found in our data can be explained by variations in the absorbing column density across the face of the remnant. However, the PSPC is limited in its ability to distinguish between temperature and N_H variations, as can be seen from the shapes of the confidence regions in Figure 7. The simple band-ratio map of Figure 5 suggests that temperature variations may also be present, but on angular scales too small to obtain accurate spectral information with the limited statistics available from these data. We expect that observations of this object by *Asuka*, which has sufficient energy resolution to distinguish between absorption and temperature variations, would permit more detailed investigations of this very interesting object.

This work was supported by NASA grant NAG 5-1535. We are grateful to T. Landecker for providing a digital radio image of VRO 42.05.01 for comparison with our X-ray data, and for helpful comments on the manuscript by Rob Petre and by an anonymous referee. Portions of our analysis were performed with the IRAF/PROS software and with an IDL package developed by our group at Penn State. The images presented here were produced using the IPAC image processing package s.X on a Sun workstation.

REFERENCES

Bloemen, J. B. G. M. 1987, ApJ, 322, 694
Bohlin, R. C., Savage, B. D., & Drake, J. F. 1978, ApJ, 224, 132
Burrows, D. N., Singh, K. P., Nousek, J. A., Garmire, G. P., & Good, J. 1993, ApJ, 406, 97
D'Odorico, S., & Sabbadin, F. 1977, A&AS, 28, 439
Fesen, R. A., Blair, W. P., & Kirshner, R. P. 1985, ApJ, 292, 29
Fesen, R. A., Gull, T. R., & Ketelsen, D. A. 1983, ApJS, 51, 337
Hamilton, A. J. S., Sarazin, C. L., & Chevalier, R. A. 1983, ApJS, 51, 115 (HSC83)
Haslam, C. G. T., & Salter, C. J. 1971, MNRAS, 151, 385
Landecker, T. L.. Pineault, S., Routledge, D., & Vaneldik, J. F. 1982, ApJ, 261, L41
———. 1989, MNRAS, 237, 277
Lozinskaya, T. A. 1975, Soviet Astron., 19, 21
———. 1979, Australian J. Phys., 32, 113
Lucke, P. B. 1978, A&A, 64, 367
Pineault, S., Landecker, T. L., & Routledge, D. 1987, ApJ, 315, 580
Pineault, S., Pritchet, C. J., Landecker, T. L., Routledge, D., & Vaneldik, J. F. 1985, A&A, 151, 52
Raymond, J. C., & Smith, B. W. 1977, ApJS, 35, 419
Snowden, S. L., McCammon, D., Burrows, D. N., & Mendenhall, J. A. 1994, ApJ, in press
Tenorio-Tagle, G., Bodenheimer, P., & Yorke, H. W. 1985, A&A, 145, 70
van den Bergh, S. 1960, Z. Astrophys., 51, 15
White, R. L., & Long, K. S. 1991, ApJ, 373, 543 (WL91)
Wood, K. S., et al. 1984, ApJS, 56, 507